XVI International Conference on Computational Plasticity. Fundamentals and Applications
COMPLAS 2021
E. Oñate, D. Peric, M. Chiumenti and Eduardo de Souza Neto (Eds)

HOMOGENIZATION OF MESOSCALE DISCRETE MODEL FOR POROELASTICITY

JAN ELIÁŠ[*] AND GIANLUCA CUSATIS[†]

[*] Institute of Structural Mechanics
Brno University of Technology
Veveří 95, 602 00 Brno, Czech Republic
e-mail: jan.elias@vut.cz

[†] Department of Civil and Environmental Engineering
Northwestern University
2145 Sheridan Road, Evanston, IL 60208-310, USA
e-mail: g-cusatis@northwestern.edu

Key words: Homogenization, poroleasticity, discrete model, Biot's theory

Abstract. Biot's theory of coupled mechanical-transport behavior of porous materials is applied in the framework of discrete mesoscale modeling. The contribution presents asymptotic expansion homogenization of the discrete poromechanical model. The macroscale becomes homogeneous and continuous and contains all the coupling effects. In contrast, the microscale is discrete and completely decoupled, separate representative volume elements (RVEs) appear for mechanical and mass transport problems. Linear elastic material behavior is assumed, therefore response of the RVEs can be pre-computed in advance and used repetitively at integration points of the macroscopic model.

1 INTRODUCTION

Robust computational models of concrete relies often on detailed representation of its mesostructure (aggregates, matrix, pores, interfaces). Thus, they are computationally demanding. The contribution uses discrete mesoscale models of concrete where each rigid particle of the model corresponds to one larger mineral aggregate and contacts represent matrix between them. Even such efficient mesostructure representation results in computational burden whenever larger material volumes needs to be simulated. For examples, simulation of bent reinforced concrete beam by Lattice-Discrete Particle Model (LDPM, [1]) is arguably the largest structural member analyzed with such modeling technique [2].

Rezakhani and Cusatis [3] developed homogenized description of the discrete model via asymptotic expansion. This computational homogenization technique replaces macroscopic constitutive relations by "virtual experiment". Each macroscopic integration point is connected to a representative volume element (RVE) where detailed discrete mesoscale model is loaded by macroscopic strain quantities, analyzed and provides corresponding macroscopic stresses.

Motivated by excellent result of the discrete models in simulations of coupling mechanics and mass transport [4, 5, 6], we now extend this homogenization for the coupled model. The present contribution is limited to poroelasticity, The originally coupled mesoscale model breaks down by homogenization into independent system of two RVEs. One RVE is purely mechanical, the second RVE is used for transport. Coupling terms binding this two RVEs together appear at the macroscale only.

The contribution briefly presents the mathematical derivation of the homogenization and simple example of Terzaghi's consolidation verifying the developed equations.

2 DISCRETE MESOSCALE MODEL OF HETEROGENEOUS MATERIAL

Model geometry is created by placing virtual spherical grains randomly into a volume with no overlapping. These grains represent mineral aggregates, their diameters are generated by Fuller curve. Power tessellation is performed on these spheres, giving rise to convex polyhedrons encapsulating each sphere. The polyhedrons are considered ideally rigid, contacts between them are compliant and account for elastic behavior of the material. Delaunay triangulation, the dual object to the tessellation, provides conduit elements for the transport part of the model.

The model has three master fields: pressure p, displacement vector $\boldsymbol{u}$, and rotation vector $\boldsymbol{\theta}$. The pressure is defined at the vertices P, Q, ... of the power tessellation while the displacements and rotations are defined at the centroids I, J, ... of grains.

The first set of model equations defines pressure gradient g and strain vector $\boldsymbol{\varepsilon}$.

$$g = \frac{p^Q - p^P}{h} \tag{1a}$$

$$\varepsilon_\alpha = \frac{1}{l}\left(\boldsymbol{u}^J - \boldsymbol{u}^I + \boldsymbol{\mathcal{E}} : (\boldsymbol{\theta}^J \otimes \boldsymbol{c}_J - \boldsymbol{\theta}^I \otimes \boldsymbol{c}_I)\right) \cdot \boldsymbol{e}_\alpha \tag{1b}$$

where h and l are length of conduit and mechanical elements, respectively. $\boldsymbol{c}_I$ or $\boldsymbol{c}_j$ are vectors connecting nodes I or J with the centroid of the face of mechanical element IJ. $\boldsymbol{e}_\alpha$ with $\alpha \in (N, M, L)$ are unit normal and tangential vectors at the face of the mechanical element. $\boldsymbol{\mathcal{E}}$ is the Levi-Civita permutation tensor.

The second set of constitutive equations defines flux density j and traction $\boldsymbol{t}$

$$j = -\lambda g \tag{2a}$$

$$t_\alpha = E_\alpha \varepsilon_\alpha - b p_a \boldsymbol{e}_N \cdot \boldsymbol{e}_\alpha \tag{2b}$$

with λ and b being the permeability coefficient (hydraulic conductivity) and Biot coefficient, respectively. E_α are contact elastic parameters, p_a is average pressure in the mechanical element. Some discrete models consider also a bending moment at the contact faces due to curvature, but it is omitted here for sake of simplicity.

Finally, the third equation set brings the balance equations for nodes P (mass transport) and I (mechanics).

$$\rho\left(3b\dot{\epsilon}_V - \frac{p}{M_b}\right)W + Wq = \sum_Q Sj \tag{3a}$$

$$-V\boldsymbol{b} = \sum_J At_\alpha \boldsymbol{e}_\alpha \tag{3b}$$

$$\boldsymbol{0} = \sum_J A\boldsymbol{w} \tag{3c}$$

where Q and J visits all the neighbors of P and I, respectively. The second and third equations are static equilibrium equations of forces and moments. The first equation expresses mass balance of fluid. ρ is fluid density, $\dot{\epsilon}_V$ is time derivative of volumetric strain, M_b is Biot modulus, S and A are areas of the conduit and mechanical elements, respectively. W is volume of Delaunay simplex corresponding to node P, V is volume of power region corresponding to node I. $\boldsymbol{w} = \boldsymbol{\mathcal{E}} : (\boldsymbol{c}_I \otimes \boldsymbol{t})$ is the moment of traction.

3 SCALE SEPARATION

We now perform scale separation of the governing equations. The global macroscopic reference system is X. At every point of the macroscale, we define local macroscopic reference system $\boldsymbol{x}$. There is also local microscale reference system $\boldsymbol{y}$ with the following relation to $\boldsymbol{x}$

$$\boldsymbol{x} = \eta\boldsymbol{y} \tag{4}$$

η being the separation of scales constant.

The master field is decomposed into

$$p(\boldsymbol{X},\boldsymbol{y}) = p^{(0)}(\boldsymbol{X},\boldsymbol{y}) + \eta p^{(1)}(\boldsymbol{X},\boldsymbol{y}) + \dots \tag{5a}$$

$$\boldsymbol{u}(\boldsymbol{X},\boldsymbol{y}) = \boldsymbol{u}^{(0)}(\boldsymbol{X},\boldsymbol{y}) + \eta\boldsymbol{u}^{(1)}(\boldsymbol{X},\boldsymbol{y}) + \dots \tag{5b}$$

$$\boldsymbol{\theta}(\boldsymbol{X},\boldsymbol{y}) = \eta^{-1}\boldsymbol{\omega}^{(-1)}(\boldsymbol{X},\boldsymbol{y}) + \boldsymbol{\omega}^{(0)}(\boldsymbol{X},\boldsymbol{y}) + \boldsymbol{\varphi}^{(0)}(\boldsymbol{X},\boldsymbol{y}) + \eta\boldsymbol{\varphi}^{(1)}(\boldsymbol{X},\boldsymbol{y}) + \dots \tag{5c}$$

The expansion of the rotation follows from [3].

Neighboring nodes P and Q as well as I and J are, from the viewpoint of the macroscopic variable $\boldsymbol{X}$, close to each other. We can, according fo [7], approximate the master fields at points Q and J by Taylor expansion series at points P and I, respectively.

$$p(\boldsymbol{X}_Q,\boldsymbol{y}_Q) = p(\boldsymbol{X}_P,\boldsymbol{y}_Q) + \frac{\partial p(\boldsymbol{X}_P,\boldsymbol{y}_Q)}{\partial X_i}x_i^{PQ} + \frac{1}{2}\frac{\partial^2 p(\boldsymbol{X}_P,\boldsymbol{y}_Q)}{\partial X_i X_j}x_i^{PQ}x_j^{PQ} + \mathcal{O}(h^3) \tag{6a}$$

$$\boldsymbol{u}(\boldsymbol{X}_J,\boldsymbol{y}_J) = \boldsymbol{u}(\boldsymbol{X}_I,\boldsymbol{y}_J) + \frac{\partial \boldsymbol{u}(\boldsymbol{X}_I,\boldsymbol{y}_J)}{\partial X_j}x_j^{IJ} + \frac{1}{2}\frac{\partial^2 \boldsymbol{u}(\boldsymbol{X}_I,\boldsymbol{y}_J)}{\partial X_j X_k}x_j^{IJ}x_k^{IJ} + \mathcal{O}(l^3) \tag{6b}$$

$$\boldsymbol{\theta}(\boldsymbol{X}_J,\boldsymbol{y}_J) = \boldsymbol{\theta}(\boldsymbol{X}_I,\boldsymbol{y}_J) + \frac{\partial \boldsymbol{\theta}(\boldsymbol{X}_I,\boldsymbol{y}_J)}{\partial X_j}x_j^{IJ} + \frac{1}{2}\frac{\partial^2 \boldsymbol{\theta}(\boldsymbol{X}_I,\boldsymbol{y}_J)}{\partial X_j X_k}x_j^{IJ}x_k^{IJ} + \mathcal{O}(l^3) \tag{6c}$$

Equations (5) and (6) are now substituted into the balance equations (3). These equations are then transformed into $\boldsymbol{y}$ reference system and terms with the same η power are collected together. Three highest powers of η are considered for further analysis:

η^{-3} We derive at this level, after some mathematical work, that (i) pressure $p^{(0)}$ is constant over the RVE, (ii) rotation $\eta^{-1}\boldsymbol{\omega}^{(-1)}$ is constant over the RVE and equal to $\boldsymbol{\varphi}^{(0)}$, and (iii) translations $\boldsymbol{u}^{(0)}$ represents rigid body motion of the whole RVE. The variable $\boldsymbol{u}^{(0)}$ is therefore replaced by displacement $\boldsymbol{v}$ of the RVE centroid and its rotation $\boldsymbol{\varphi}^{(0)}$.

η^{-2} This level describes the solution of the discrete RVE problem. Load to the RVE problem comes in a form of eigen pressure gradient and eigen strain obtained as projections of the macroscopic pressure gradient, macroscopic strain, and macroscopic curvature. The periodic boundary conditions are applied. Degrees of freedom are $\eta p^{(1)}$, $\eta\boldsymbol{u}^{(1)}$ and $\boldsymbol{\omega}^{(0)}$. Transport problem is always steady state and completely decoupled from the mechanical one. One can solve the transport and mechanical RVE independently. Since they are linear, it is easy to pre-compute the RVE response at the beginning and use this pre-computed results at all integration points during the macroscale simulation.

η^{-1} This level provides the macroscopic solution. After several mathematical operations, one arrives at definition of the following tensors

$$\boldsymbol{f} = \frac{1}{V_0}\sum_{e\in V_0} hS\lambda g^{(0)}\boldsymbol{e}_\lambda \tag{7a}$$

$$\boldsymbol{\sigma}_\mathrm{s} = \frac{1}{V_0}\sum_{e\in V_0} lAE_\alpha\varepsilon_\alpha^{(0)}\boldsymbol{e}_N\otimes\boldsymbol{e}_\alpha \tag{7b}$$

$$\boldsymbol{\mu}_\mathrm{s} = \frac{1}{V_0}\sum_{e\in V_0} lA\boldsymbol{e}_N\otimes\left(E_\alpha\varepsilon_\alpha^{(0)}\boldsymbol{\mathcal{E}}:(\boldsymbol{x}^c\otimes\boldsymbol{e}_\alpha)\right) \tag{7c}$$

$$\boldsymbol{\xi} = \frac{1}{V_0}\sum_{e\in V_0} lAb\boldsymbol{e}_N\otimes\boldsymbol{e}_N \tag{7d}$$

$$\boldsymbol{\zeta} = \frac{1}{V_0}\sum_{e\in V_0} lAb\boldsymbol{e}_N\otimes(\boldsymbol{\mathcal{E}}:(\boldsymbol{x}^c\otimes\boldsymbol{e}_N)) \tag{7e}$$

V_0 is the RVE volume and $\boldsymbol{x}^c$ is the centroid of the mechanical element face. The obtain tensors collect information from the RVE and bring is back to the macroscale. $\boldsymbol{f}$ is a vector of macroscopic fluxes, $\boldsymbol{\sigma}_s$ is macroscopic, generally non-symmetric stress tensor of the solid, $\boldsymbol{\mu}_s$ is macroscopic couple stress tensor of the solid, $\boldsymbol{\xi}$ and $\boldsymbol{\zeta}$ are auxiliary tensors used to calculate effect of pressure on macroscopic stress and couple stress.

These quantities than appears in macroscopic balance equations derived at this level.

$$\nabla_X\cdot\boldsymbol{f} = \rho\left(3b\dot{\epsilon}_V^{(0)} + \frac{\dot{p}^{(0)}}{M_b}\right) + q \tag{8a}$$

$$\nabla_X\cdot\boldsymbol{\sigma}_\mathrm{s} - \nabla_X p^{(0)}\cdot\boldsymbol{\xi} = -\boldsymbol{b} \tag{8b}$$

$$\nabla_X\cdot\boldsymbol{\mu}_\mathrm{s} - \nabla_X p^{(0)}\cdot\boldsymbol{\zeta} + \boldsymbol{\mathcal{E}}:\boldsymbol{\sigma}_\mathrm{s} - p^{(0)}\boldsymbol{\mathcal{E}}:\boldsymbol{\xi} = \boldsymbol{0} \tag{8c}$$

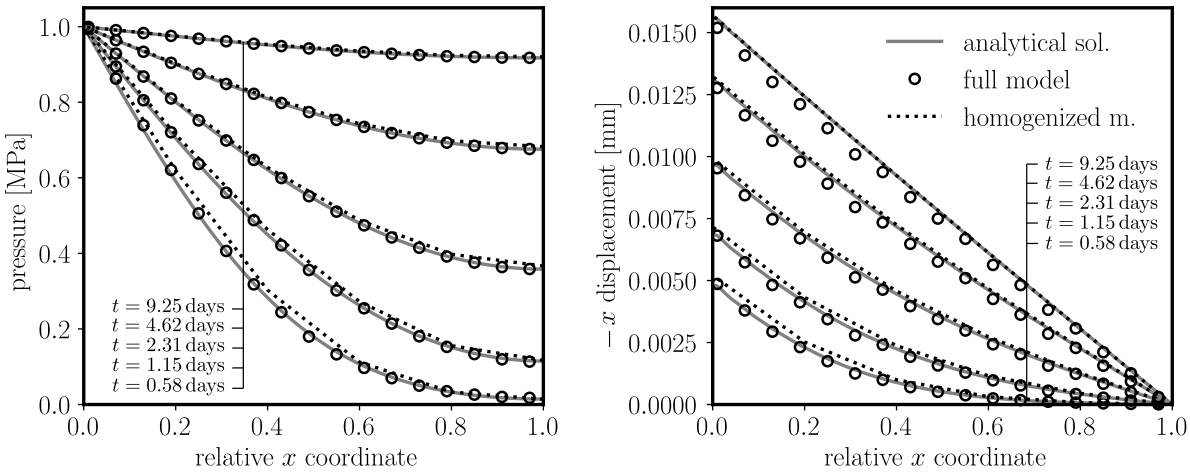

Figure 1: Results of the *full* and *homogenized* models as well as analytical solution. Pressure and x displacement profiles along the central axis of the specimen at various time instants.

The fist two equations correspond to classical poroelasticity of Cauchy continuum, while the last equation brings Cosserat effects.

4 VERIFICATION

The model is verified by simulating Terzaghi's consolidation. A prism of material of size $0.5 \times 0.1 \times 0.1\,\mathrm{m}^3$ is initially under zero pressure and zeros strain. The x axis runs along its longest central axis, the domain begins at $x = 0\,\mathrm{m}$ and ends at $x = 0.5\,\mathrm{m}$. The prism is sealed at all boundaries except the front end at $x = 0$ where pressure $p^\star = 1\,\mathrm{MPa}$ is applied at time $t = 0$. The mechanical boundary conditions prescribe zero rotations at all boundaries, zero x displacement at rear end at $x = 0.5\,\mathrm{m}$ and zero y and z displacements at all rectangular sides. Material parameters are the following: $E_N = 21.5\,\mathrm{GPa}$, $E_M = E_L = 6.45\,\mathrm{GPa}$, $\rho = 1000\,\mathrm{kg/m}^3$, $b = 0.5$, $\lambda = 5.62 \times 10^{-12}\,\mathrm{s}$ and $M_b = 0.61 \times 10^8\,\mathrm{Pa}$.

We simulated the problem using the *full* discrete model ($l_{\min} = 0.02\,\mathrm{m}$) and *homogenized* continuous model. We used 5 trilinear 8-node isoparametric finite elements along the specimen x direction. Comparison of both models in terms of pressure and x displacement profile along the central x axis at different time instant is presented in Fig. 1. Differences are attributed to (i) heterogeneity and (ii) boundary layer effect [8], or wall effect, that is present in the *full* model and modify the mechanical properties in the vicinity of the boundary.

There exists an analytical solution to the problem [9, 10]. Pressure and displacement

is provided by the following functions

$$p(\chi,\tau) = p^\star \left[1 - \sum_{m=1,3,\ldots}^{\infty} \frac{4}{m\pi} \sin\left(\frac{m\pi\chi}{2}\right) \exp\left(-m^2\pi^2\tau\right)\right] \tag{9}$$

$$u_x(\chi,\tau) = -\frac{np^\star l}{G}\left[\sum_{m=1,3,\ldots}^{\infty} \frac{8}{m^2\pi^2} \cos\left(\frac{m\pi\chi}{2}\right)\left[1 - \exp\left(-m^2\pi^2\tau\right)\right]\right] \tag{10}$$

where $\chi = x/l$, $\tau = \lambda t/4Cl^2$, $n = b(1-2\nu)/(2(1-\nu))$, $l = 0.5\,\mathrm{m}$, $G = E/2(1+\nu)$, $C = (1-\nu_u)(1-2\nu)/(M_b(1-\nu)(1-2\nu_u))$, $\nu_u = (3K_u - 2G)/2(3K_u + G)$ and $K_u = M_b b^2 + E/3(1-2\nu)$. $E = 13.97\,\mathrm{GPa}$ and $\nu = 0.175$ being macroscopic elastic parameters estimated based on the RVE response. The analytical solution agrees reasonably well with the model results.

5 CONCLUSIONS

Discrete model of coupled mass transport and mechanics is homogenized using asymptotic expansion. The coupling between transport and mechanical parts according to the Biot's theory takes places at the macroscale only. The microscale, featuring periodic response of RVE, is completely decoupled. The RVE problem for mechanics and transport is therefore solved separately. Thanks to consideration of linear elastic behavior, RVE responses can be pre-computed in advance to speed up the simulation.

Verification of the homogenized model was done on a simple example of Terzaghi's consolidation. Simulation of a prism loaded by an abrupt change in surface pressure shows reasonable correspondence of the *full* and *homogenized* models as well as the analytical solution.

ACKOWLEDGEMENT

Jan Eliáš gratefully acknowledges financial support from the Czech Science Foundation under project no. GA19-12197S.

REFERENCES

[1] Cusatis, G., Pelessone, D., and Mencarelli, A., "Lattice discrete particle model (LDPM) for failure behavior of concrete. i: Theory," *Cement & Concrete Composites*, vol. 33, no. 9, pp. 881–890, 2011.

[2] Alnaggar, M., Pelessone, D., and Cusatis, G., "Lattice discrete particle modeling of reinforced concrete flexural behavior," *Journal of Structural Engineering*, vol. 145, no. 1, p. 04 018 231, 2019.

[3] Rezakhani, R. and Cusatis, G., "Asymptotic expansion homogenization of discrete fine-scale models with rotational degrees of freedom for the simulation of quasi-brittle materials," *Journal of the Mechanics and Physics of Solids*, vol. 88, pp. 320–345, 2016.

[4] Nakamura, H., Worapong, S., Yashiro, R., and Kunieda, M., "Time-dependent structural analysis considering mass transfer to evaluate deterioration processes of RC structures," *Journal of Advanced Concrete Technology*, vol. 4, no. 1, pp. 147–158, 2006.

[5] Grassl, P., "A lattice approach to model flow in cracked concrete," *Cement and Concrete Composites*, vol. 31, no. 7, pp. 454–460, 2009.

[6] Grassl, P. and Bolander, J., "Three-dimensional network model for coupling of fracture and mass transport in quasi-brittle geomaterials," *Materials*, vol. 9, no. 9, 2016.

[7] Fish, J., Chen, W., and Li, R., "Generalized mathematical homogenization of atomistic media at finite temperatures in three dimensions," *Computer Methods in Applied Mechanics and Engineering*, vol. 196, no. 4, pp. 908–922, 2007.

[8] Eliáš, J., "Boundary layer effect on behavior of discrete models," *Materials*, vol. 10, p. 157, 2017.

[9] Terzaghi, K., "Die berechnung der durchlassigkeitsziffer des tones aus dem verlauf der hidrodynamichen span-nungserscheinungen akademie der wissenschaften in wien," *Mathematish-Naturwissen-Schaftiliche Klasse*, vol. 132, pp. 125–138, 1925.

[10] Detournay, E. and Cheng, A. H.-D., "Fundamentals of poroelasticity," in *Analysis and Design Methods*, C. Fairhusrt, Ed., Oxford: Pergamon, 1993, pp. 113–171.